A NOVEL INTRINSIC UNSCENTED KALMAN FILTER FOR TRACTOGRAPHY FROM HARDI*

G. Cheng[1] H. Salehian[1] M. S. Hwang[2,5] D. Howland[2,5,6] J. R. Forder[3,4,5] B. C. Vemuri[1†]

[1]Dept. of CISE, [2]Neurosci., [3]Radiology and [4]Biomedical Engineering
[5]McKnight Brain Inst., [6]Brain Rehab & Res Ctr, NF/SG Veteran's Health
University of Florida, Gainesville, FL 32611, United States

ABSTRACT

The unscented Kalman filter (UKF) was recently introduced in literature for simultaneous multi-tensor estimation and tractography. This UKF however was not intrinsic to the space of diffusion tensors. Lack of this key property leads to inaccuracies in the multi-tensor estimation as well as in tractography. In this paper, we propose an novel intrinsic unscented Kalman filter (IUKF) in the space of symmetric positive definite matrices, which can be used for simultaneous recursive estimation of multi-tensors and tractography from diffusion weighted MR data. In addition to being more accurate, IUKF retains all the advantages of UKF for instance, multi-tensor estimation is only performed in the places where it is needed for tractography, which would be much more efficient than the two stage process involved in methods that do tracking post diffusion tensor estimation. The accuracy and effectiveness of the proposed method is demonstrated via real data experiments.

1. INTRODUCTION

Diffusion Weighted MR Imaging (DW MRI) is the technique that can measure the local constrained water diffusion properties in different spatial directions in MR signals and thus infer the underlying tissue structure. It is a unique non-invasive technique that can reveal the neural fiber structures in-vivo. The local water diffusion property can be described either via a diffusivity function or a diffusion propagator function. The diffusivity function can be estimated from the DW-MR signals and represented by a 2nd order tensor at each image voxel yielding the so called Diffusion Tensor Imaging (DTI) pioneered in [1]. It is now well known that DTI fails to accurately represent locations the data volume containing complex tissue structures such as fiber crossings. To solve this problem, several higher order models were proposed such as [2, 3, 4].

To further reveal the fibrous structures such as brain white matter, fiber tracking methods were proposed to analyze the connectivities between different regions in the brain. Existing fiber tracking methods fall mainly in two categories, deterministic and probabilistic. One popular deterministic tracking method is the stream line method [5, 6], where the tracking problem is tackled using a line integration. The deterministic tracking method can also based on the (Riemannian or Finsler) geometry imposed by the diffusivity function [7] where the tracking problem is posed as a shortest path problem. In probabilistic fiber tracking methods [8, 9, 10], a probabilistic dynamic model is first built and then a filtering technique such as particle filter is applied. Most of the existing fiber tracking methods are based on two stages namely, first estimating the tensors from DWI and then tracking using these estimated tensors.

Recently, in [11] a filtered multi-tensor tractography method was proposed in which the fiber tracking and the multi-tensor reconstruction was performed simultaneously. There are mainly two advantages of this approach: (1) The reconstruction is performed only at locations where it is necessary, which would significantly reduce the computational complexity compared to the approaches that first reconstruct whole tensor field and then apply tractography, (2) fiber tracking is used as a regularization in the reconstruction i.e., the smoothness of the fiber path is used to regularize the reconstruction. However, in [11] the filtering is applied only to the tensor features (major eigen vectors etc.) all of which have strict mathematical constraints that ought to be satisfied but not all of the constraints were enforced. For example, the constraint on eigen vectors to lie on the unit sphere was not enforced. In general it would be more favorable to track the full tensor and enforce the necessary constraints. It is known that diffusion tensors are in the the space of symmetric positive definite(SPD) matrices denoted as P_n, which is not a Euclidean space but a Riemannian manifold. Vector operations are not available on P_n. So algorithms that are based on vector operations can not be applied directly to these spaces, and non-trivial extensions are needed. In this paper, we propose a novel intrinsic unscented Kalman filter on P_n, *which to the best of our knowledge is the first extension of the unscented Kalman filter to* P_n. We apply this filter to

This research was funded by the NIH grant NS066340 to BCV.
† indicates the corresponding author.

both estimate and track the tensors in the multi-tensor model using the intrinsic formulation to achieve better accuracy as demonstrated through experiments. We perform real data experiments to demonstrate the accuracy and efficiency of our method.

The rest of the paper is organized as follows: the intrinsic unscented Kalman filter is described in section 2, where in subsection 2.1 the basic geometric properties are briefly introduced, followed by a novel dynamic model defined for the multi-tensor model. We then present the intrinsic unscented Kalman filter algorithm and finally the experiments are presented in 3.

2. INTRINSIC UNSCENTED KALMAN FILTER FOR DIFFUSION TENSORS

In this section, we will describe an intrinsic unscented Kalman filter to track diffusion tensors which lie in the in the space of $n \times n$ symmetric positive definite(SPD) matrices denoted by P_n. Firstly, we will give a brief introduction of Riemannian geometry on P_n and the readers are referred to [12] for further details. The dynamic model and a novel intrinsic unscented Kalman filter based on the Riemannian geometry on P_n will then be presented in the following sections.

2.1. Riemannian Geometry on P_n

P_n, the space of $n \times n$ SPD matrices, is a smooth manifold and can be represented as a quotient space $P_n = GL(n)/O(n)$ where $GL(n)$ denotes the General Linear group (the group of $n \times n$ non-singular matrices) and $O(n)$ denotes the space of $n \times n$ orthogonal matrices. So the natural way to move on P_n is by using the GL group action. Let $\mathbf{X} \in P_n$, $\mathbf{g} \in GL(n)$, the group actiong applied to $\mathbf{X}$ is $\mathbf{X}[\mathbf{g}] = \mathbf{g}\mathbf{X}\mathbf{g}^t$. At each point $\mathbf{X} \in P_n$ there is a tangent space denoted by $T_{\mathbf{X}}P_n$ which can be identified with a vector space $Sym(n)$ – the space of $n \times n$ symmetric matrices. For tangent vectors $\mathbf{U}$ and $\mathbf{V} \in T_{\mathbf{X}}P_n$ the intrinsic inner-product/metric can be defined as

$$< \mathbf{U}, \mathbf{V} >_X = tr(\mathbf{X}^{-1/2} U \mathbf{X}^{-1} V \mathbf{X}^{-1/2}). \tag{1}$$

With this metric the distance between two points $\mathbf{X}, \mathbf{Y} \in P_n$ can be defined as the length of the geodesic in the manifold between $\mathbf{X}, \mathbf{Y}$, which can be written in a closed form

$$dist(\mathbf{X}, \mathbf{Y})^2 = tr(\log^2(\mathbf{X}^{-1}\mathbf{Y})) \tag{2}$$

where $\log$ is the matrix log function. The exponential map in P_n at a certain point $\mathbf{X} \in P_n$ denoted by $Exp_{\mathbf{X}}(\cdot)$ maps a tangent vector $\mathbf{V} \in T_{\mathbf{X}}P_n$ rooted at the origin to a geodesic in the manifold. That is, the curve segment $\gamma(t) = Exp_{\mathbf{X}}(t\mathbf{V}), t \in [0, 1]$ is a geodesic from $\gamma(0) = \mathbf{X}$ to $Exp_{\mathbf{X}}(\mathbf{V})$. The Log map ($Log_{\mathbf{X}}(\cdot)$) is the inverse of the Exponential map. The Exponential and Log map on P_n are given by $Exp_{\mathbf{X}}(\mathbf{V}) = \mathbf{X}^{1/2} \exp(\mathbf{X}^{-1/2}\mathbf{V}\mathbf{X}^{-1/2})\mathbf{X}^{1/2}$and $Log_{\mathbf{X}}(\mathbf{Y}) = \mathbf{X}^{1/2} \log(\mathbf{X}^{-1/2}\mathbf{Y}\mathbf{X}^{-1/2})\mathbf{X}^{1/2}$ where $\mathbf{X}, \mathbf{Y} \in P_n$, $\mathbf{V} \in T_{\mathbf{X}}P_n$, and log and exp denote the matrix exp and log operators.

The extension of the arithmetic mean in the Euclidean space to the Riemannian manifold is the Karcher mean – an estimator that minimizes the sum of squared distances. In P_n the Karcher mean of set of elements $\mathbf{X}_i \in P_n$ is

$$\mu^* = \widehat{\sum}_i \mathbf{X}_i = argmin_\mu \sum_i dist^2(\mathbf{X}_i, \mu) \tag{3}$$

This optimization can be computed using a gradient based technique.

For a certain matrix-valued random variable $\mathbf{X} \in P_n$, the intrinsic expectation can be defined similarly to the Karcher mean,

$$E(\mathbf{X}) = argmin_{\mathbf{Y}} \int_{P_n} dist^2(\mathbf{X}, \mathbf{Y}) \mathbf{dP}(\mathbf{X}) \tag{4}$$

, where $dP(X)$ is the probability measure. This expectation is called Karcher expectation. The matrix-valued random variable $\mathbf{X}$ can then be projected to $T_{E(\mathbf{X})}P_n$, and the covariance matrix can be defined in this tangent space.

2.2. The State Transition and Observation Models

The state transition model on P_n in this paper is based on the GL operation and the LogNormal distribution. For the bi-tensor (sum of two Gaussians) model, the state transition model at step k is given by,

$$\begin{aligned} \mathbf{D}_{k+1}^{(1)} &= Exp_{\mathbf{F}\mathbf{D}_k^{(1)}\mathbf{F}^t}(\mathbf{v}_k^{(1)}) \\ \mathbf{D}_{k+1}^{(2)} &= Exp_{\mathbf{F}\mathbf{D}_k^{(2)}\mathbf{F}^t}(\mathbf{v}_k^{(2)}) \end{aligned} \tag{5}$$

where, $\mathbf{D}_k^{(1)}$, $\mathbf{D}_k^{(2)}$ are the two tensor states at step k, $\mathbf{F}$ is the state transition GL based operation, $\mathbf{v_k^{(1)}}$ and $\mathbf{v_k^{(2)}}$ are the Gaussian distributed state transition noise for $\mathbf{D}_k^{(1)}$ and $\mathbf{D}_k^{(2)}$ in the tangent space $T_{\mathbf{D}_k^{(1)}}P_3$ and $T_{\mathbf{D}_k^{(2)}}P_3$ respectively. Here we assume that the two state transition noise models are independent from each other and the previous states. The covariance matrices of the two state transition noise models are $\mathbf{Q}_k^{(1)}$ and $\mathbf{Q}_k^{(2)}$ respectively. The covariance matrix $\mathbf{Q}_k^{(i)}$ $i = 1, 2$ is a 6×6 matrix defined for the tangent vectors in $T_{\mathbf{D}_k^{(1)}}P_3$. Note that $\mathbf{Q}_k^{(i)}$ is not invariant to GL coordinate transform on P_n. Assume a random variable $\mathbf{X} = Exp_\mu(\mathbf{v})$ in P_n, where $\mathbf{v}$ is a random vector from a zero mean Gaussian with $\mathbf{Q}$ being the covariance matrix. Then, after a GL coordinate transform $\mathbf{g} \in GL(n)$, the new random variable $\mathbf{Y} = \mathbf{g}\mathbf{X}\mathbf{g}^t = Exp_{\mathbf{g}\mu\mathbf{g}^t}(\mathbf{u})$. The covariance matrix of $\mathbf{u}$ is

$$\mathbf{Q}(\mathbf{g}) = (\mathbf{g} \otimes \mathbf{g})^{-1} \mathbf{Q} (\mathbf{g} \otimes \mathbf{g})^{-t} \tag{6}$$

where $\otimes$ denotes the Kronecker product. In this paper, we first define the covariance matrix at the identity $\mathbf{Q}_{\mathbf{I}_{3\times 3}} = q\mathbf{I}_{6\times 6}$, where q is a positive scalar. And the covariance matrix at point $\mathbf{X}$ can be computed using Eq. 6 by setting $\mathbf{g} = \mathbf{X}^{\frac{1}{2}}$. With this definition the state transition noise is independent with respect to the system state.

The observation model is based on the bi-tensor diffusion model.

$$S_k^{(n)} = S_0(e^{-b_n \mathbf{g}_n^t \mathbf{D}_k^{(1)} \mathbf{g}_n^t} + e^{-b_n \mathbf{g}_n^t \mathbf{D}_k^{(2)} \mathbf{g}_n^t}) \quad (7)$$

where $\mathbf{g}_n$ denotes the direction of n-th magnetic gradient, and b_n is the corresponding b-value, and $S_k^{(n)}$ is the MR signal for n-th gradient at iteration step k. The covariance matrix of the observation model for all the magnetic gradients is a diagonal matrix denoted by $\mathbf{R}$. This assumes that the measurements from distinct gradient directions are independent.

2.3. The Intrinsic Unscented Kalman Filter

Just as in the standard Kalman filter, at each iteration step of the unscented Kalman filter [11] there are two stages, the prediction and update stages respectively. In the prediction stage, the state of the filter at the current iteration is predicted based on the result from the previous step and the state transition model. In the update step, the information from the observation at the current iteration is used in the form of the likelihood to correct the prediction. Since the states are now diffusion tensors which are in the space of P_n, where no vector operations are available, we need a non-trivial extension of the Unscented Kalman filter, especially for the prediction stage to be valid on P_n.

To begin with, we define the augmented state for the bi-(diffusion) tensor state at iteration step k to be

$$\mathbf{X}_k = [\mathbf{u}_k^{(1),t}, \mathbf{u}_k^{(2),t}, \mathbf{v}_k^{(1),t}, \mathbf{v}_k^{(2),t}]^t \quad (8)$$

where $\mathbf{v}_k^{(i)}$ $i = 1, 2$ is the state transition noise vector for diffusion tensor state $\mathbf{D}_k^{(i)}$ and $\mathbf{u}_k^{(i)} = Log_{E_{\mathbf{K}}(\mathbf{D}_k^{(i)})}(\mathbf{D}_k^{(i)})$ which is the representation of the state random variable in the tangent plane at its Karcher expectation($E_{\mathbf{K}}(\cdot)$). $\mathbf{X}_k$ is zero mean and with covariance matrix denoted by $\mathbf{P}_k^a$. The covariance matrix for the state $[\mathbf{u}_k^{(1),t}, \mathbf{u}_k^{(2),t}]^t$ is denoted by $\mathbf{P}_{k,DD}$. Note that $\mathbf{P}_k^a$ is a block-wise diagonal matrix composed from $\mathbf{P}_{k,DD}$, $\mathbf{Q}_k^{(1)}$ and $\mathbf{Q}_k^{(2)}$.

In the prediction stage, $2L+1$ weighted samples from the distribution of $\mathbf{X}_k^t$ are first computed by a deterministic sampling scheme given below. Here, $L = 24$ and denotes the dimension of $\mathbf{X}_k^t$.

$$\mathcal{X}_{k,0} = 0, \qquad w_0 = \kappa/(L+\kappa) \quad (9)$$

$$\mathcal{X}_{k,j} = (\sqrt{(L+\kappa)\mathbf{P}_k^a})_j, \qquad w_j = 1/2(L+\kappa) \quad (10)$$

$$\mathcal{X}_{k,j+L} = -(\sqrt{(L+\kappa)\mathbf{P}_k^a})_j, \quad w_{j+n} = 1/2(L+\kappa) \quad (11)$$

where w_j is the weight for the corresponding sample, $\kappa \in R$ is a parameter to control the scatter of the samples, and $(\sqrt{(L+\kappa)\mathbf{P}_k^a})_j$ is the j-th column vector of matrix $\sqrt{(L+\kappa)\mathbf{P}_k^a}$. Since samples $\mathcal{X}_{k,j} = [\mathbf{u}_{k,j}^{(1),t}, \mathbf{u}_{k,j}^{(2),t}, \mathbf{v}_{k,j}^{(1),t}, \mathbf{v}_{k,j}^{(2),t}]^t$ are generated from the joint distribution of posterior and state transition at frame k, we can get the samples from the distribution of prediction in frame $k+1$ based on $\mathcal{X}_{k,j}$ through a two-step procedure. First we can get the samples from the posterior $\mathbf{D}_{k,j}^{(i)} = Exp_{\hat{\mathbf{D}}_k^{(i)}}(\mathbf{u}_{k,j}^{(i)})$ where $\hat{\mathbf{D}}_k^{(i)}$ is the state estimate from the last iteration (the estimator of $E_{\mathbf{K}}(\mathbf{D}_k^{(i)})$). And then the samples from the predicted distribution can be generated based on $\mathbf{D}_{k,j}^{(i)}$ and $\mathbf{v}_{k,j}^{(i)}$, $\mathcal{D}_{k+1,j}^{(i)} = Exp_{\mathbf{D}_{k,j}^{(i)}}(\mathbf{v}_{k,j}^{(i)})$ where $\mathcal{D}_{k+1,j}^{(i)}$ denotes the j-th sample from the distribution of the prediction. The predicted mean is computed as the weighted Karcher mean, $\hat{\mathcal{D}}_{k+1}^{(i)} = \widehat{\sum_j} w_j \mathcal{D}_{k+1,j}^{(i)}$ The predicted covariance of the states is computed in the product space $T_{\hat{\mathcal{D}}_{k+1}^{(1)}} P_3 \times T_{\hat{\mathcal{D}}_{k+1}^{(2)}} P_3$, $\mathcal{P}_{k+1,\mathbf{DD}} = \sum_j w_j \mathcal{U}_j \mathcal{U}_j^t$ where $\mathcal{U}_j^t = [Log_{\hat{\mathcal{D}}_{k+1}^{(1)}}(\mathcal{D}_{k+1,j}^{(1)}), Log_{\hat{\mathcal{D}}_{k+1}^{(2)}}(\mathcal{D}_{k+1,j}^{(2)})]$ is a concatenation of the two vectors obtained from the Log-map of each predicted sample.

Applying the observation model defined in Equation 7 to the predicted state samples we get the predicted vector of MR signals for different magnetic gradients denoted by $\mathcal{S}_{k+1,j}$. Because this is in a vector space, we can use standard vector operations to compute the predicted mean $\hat{\mathcal{S}}_{k+1}$ as the average of $\mathcal{S}_{k+1,j}$. Using the observation noise covariance $\mathbf{R}$, the predicted observation covariance can be computed as $\mathcal{P}_{k+1,\mathbf{SS}} = \mathbf{R} + \sum_j w_j(\mathcal{S}_{k+1,j} - \hat{\mathcal{S}}_{k+1})(\mathcal{S}_{k+1,j} - \hat{\mathcal{S}}_{k+1})^t$. Also the cross-correlation matrix between the observation and the states is given by, $\mathcal{P}_{k+1,\mathbf{DS}} = \sum_j w_j(\mathcal{U}_j(\mathcal{S}_{k+1,j} - \hat{\mathcal{S}}_{k+1})^t)$

In the update step, the Kalman gain is computed as $\mathcal{K}_{k+1} = \mathcal{P}_{k+1,\mathbf{DS}}\mathcal{P}_{k+1,\mathbf{SS}}^{-1}$. Knowing the Kalman gain we can update of the states and covariance which are given by: $\hat{\mathbf{D}}_{k+1}^{(i)} = Exp_{\hat{\mathcal{D}}_{k+1}^{(i)}} \mathbf{z}_{k+1}^{(i)}$and $\mathbf{P}_{k+1,DD} = \mathcal{P}_{k+1,DD} - \mathcal{K}_{k+1}\mathcal{P}_{k,\mathbf{SS}}\mathcal{K}_{k+1}^t$where $[\mathbf{z}_{k+1}^{(1),t}, \mathbf{z}_{k+1}^{(2),t}]^t = \mathcal{K}_{k+1}(\mathbf{S}_{k+1} - \hat{\mathcal{S}}_{k+1})$, and $\mathbf{S}_{k+1}$ is the observation (MR signal vector) at step $k+1$.

3. EXPERIMENTS

To validate our tractography, we applied IUKF to HARDI scans of rat cervical spinal cord at $C3$ $C5$. In this experiment, 8 different rats were included 6 of them healthy and 2 injured with the injury in the thoracic spinal cord. The HARDI scan for each rat was acquired with 1 s0 image (taken with b closed to zero), and 21 different diffusion gradients with $b = 1000s/mm^2$, $\Delta = 13.4ms$ and $\delta = 1.8ms$. The voxel size of the scan is $35\mu m \times 35\mu m \times 300\mu m$, and the image resolution is $128x128$ in the $x-y$ plane and in the z-direction the resolution is 24 to 34. All HARDI datasets where aligned into

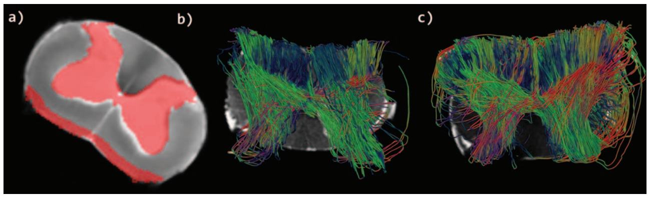

Fig. 1. Fiber tracking results on real datasets. Figure (a) is the region of interest overlayed with the S_0 image. Figure (b) & (c) are the fiber tracking result of a healthy (injured) rat overlayed on S_0 where the fibers are colored by its local direction with xyz being encoded by RGB.

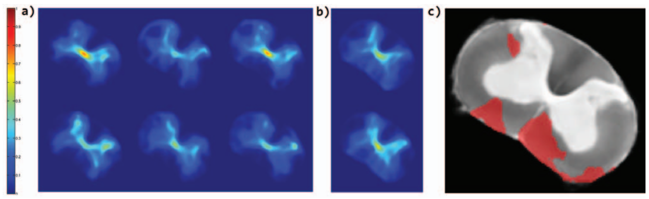

Fig. 2. Biomarkers captured by computing density map for each fiber bundle. Figure (a) & (b) show a sample slice of fiber density maps obtained for each control and injured rats, respectively. Figure (c) is the region in which the p-value is less than 0.005, overlaid on the S_0 image.

the same coordinate system by a similarity transform before tracking. To initialize the algorithm, for each scan we first placed a seed point at each voxel of the grey matter, and then a 2nd order tensor estimation is employed as an initialization for the algorithm. In the experiment, various parameters were set to: the state transition noise variance in Equation 5 $\mathbf{Q}_1 = \mathbf{Q}_2 = 0.1\mathbf{I}$, the observation noise variance $\mathbf{R} = 0.03I$ and the size of each tacking step $\delta t = 0.01mm$. The algorithm stops if the angle between two consecutive tangent vectors becomes larger than 60 degree or the fiber tract arrives at the boundary of the spinal cord.

The fiber bundle of interest is the motoneuron which starts from the gray matter and ends at the boundary of the spinal cord. To visualize the motoneuron fiber bundle, we took corresponding ROIs such that only the fiber passing through the ROIs are displayed. The results are shown in Figure 2, where we can find fiber bundles starting from the gray matter and end at the boundary of the spinal cord. The differences between the injured and control rats are not easily seen directly. To visualize the difference between the healthy and injured rats, we first computed the axonal fiber density map for each rat by counting the number of fibers passing through the 3-by-3 neighborhood of each voxel. We then non-linearly deform the density map to a spinal cord atlas derived from HARDI data [13] and do voxel-wise t-test analysis. The result are shown in the Figure 2, where we can find significant differences between the healthy and the injured rats in the motoneuron region, which demonstrates the effectiveness of our tracking method.

4. CONCLUSION

We have presented a novel intrinsic unscented Kalman filter for simultaneous estimation of multi-tensors and smooth fiber tracking. The key difference between existing unscented Kalman filter based algorithm for tractography and the method presented here is that our technique makes use of the group operations on the manifold of diffusion tensors, which is a Riemannian manifold and not a vector space and hence vector space operations if used are invalid on such a space. We tested the algorithm on several data sets including real rat spinal cords with and without injury. We also depicted the differences caused in the tracts due to the injury and quantified them via axonal density measure. Future work will involve further testing and quantification on several real data sets and statistical analysis.

References

[1] P. Basser, J. Mattiello, and D. LeBihan, “Estimation of the effective self-diffusion tensor from the NMR spin echo,” *J. Magn. Reson. B*, vol. 103, pp. 247–254, 1994.

[2] D. C. Alexander, “Maximum entropy spherical deconvolution for diffusion mri,” in *IPMI*, 2005, pp. 76–87.

[3] T. McGraw, B. C. Vemuri, B. Yezierski, and T. Mareci, “Segmentation of high angular resolution diffusion mri modeled as a field of von mises-fisher mixtures,” in *ECCV*, 2006.

[4] M. Descoteaux, E. Angelino, S. Fitzgibbons, and R. Deriche, “Apparent diffusion coefficients from high angular resolution diffusion imaging: Estimation and applications,” *MRM*, vol. 56, pp. 395–410, 2006.

[5] P. Basser, S. Pajevic, C. Pierpaoli, J. Duda, and A. Aldroubi, “In vivo fiber tractography using dt-mri data,” *MRM*, vol. 44, pp. 625–632, 2000.

[6] T. McGraw, B. Vemuri, Y. Chen, M. Rao, and T. Mareci, “Dt-mri denoising and neuronal fiber tracking,” *MedIA*, vol. 8, pp. 95–111, 2004.

[7] E. Prados, C. Lenglet, N. Wotawa, R. Deriche, O. Faugeras, and S. Soatto, “Control theory and fast marching techniques for brain connectivity mapping,” in *CVPR*, 2006.

[8] T. Behrens, H. Berg, S. Jbabdi, M. Rushworth, and M. Woolricha, “Probabilistic diffusion tractography with multiple fibre orientations: What can we gain?,” *NeuroImage*, vol. 34, pp. 144–155, 2007.

[9] F. Zhang, E. R. Hancock, C. Goodlett, and G. Gerig, “Probabilistic white matter fiber tracking using particle filtering and von misesfisher sampling,” *MedIA*, vol. 13, pp. 5–18, 2009.

[10] P. Savadjiev, Y. Rathi, J. G. Malcolm, M. E. Shenton, and C-F Westin, “A geometry-based particle filtering approach to white matter tractography.,” in *MICCAI*, 2010.

[11] J. G. Malcolm, M. E. Shenton, and Y. Rathi, “Filtered multitensor tractography,” *TMI*, vol. 29, pp. 1664–1674, 2010.

[12] P. T. Fletcher and S. Joshi, “Riemannian geometry for the statistical analysis of diffusion tensor data,” *Signal Processing*, vol. 87, pp. 250–262, 2007.

[13] G. Cheng, B. C. Vemuri, M. S. Hwang, D. Howland, and J. R. Forder, “Atlas construction for high angular resolution diffusion imaging data represented by gaussian mixture fields,” in *ISBI*, 2011.